Pressure-tuned resonance Raman scattering in $AgGaSe_2$

T. Sakuntala and Akhilesh K. Arora
Materials Science Division, Indira Gandhi Centre for Atomic Research, Kalpakkam, 603 102, T.N., India
(Received 30 October 1995)

Pressure-tuned resonance Raman scattering is investigated in the ambient and subsequent high-pressure phases of $AgGaSe_2$ up to a pressure of 165 kbar using several fixed wavelengths of argon and krypton ion lasers. The nonpolar Raman active mode of A_1 symmetry in the chalcopyrite phase exhibits resonances at 18 and 30 kbar for the incident wavelengths of 676.4 and 647.1 nm, respectively. From the observed resonances, the pressure coefficient of a direct interband transition involving a defect level is estimated to be 6.9 meV/kbar in the chalcopyrite phase. The observed resonances are fitted to those calculated incorporating the corrections for absorption and reflection. In the high-pressure orthorhombic phase above 51 kbar, $AgGaSe_2$ has an indirect gap that is lower than the energy of the visible photon; however, enhancement of the intensities of Raman modes is observed with yellow-green wavelengths due to resonance with another direct interband transition. The pressure coefficient of this transition in the opaque phases is found to be smaller than that in the chalcopyrite phase. [S0163-1829(96)01423-3]

I. INTRODUCTION

Resonance Raman scattering (RRS) has been used extensively to probe the electronic band structure of semiconductors and to obtain information about the electron-phonon interactions such as deformation potential and Fröhlich interaction.[1] In this context, investigations on tetrahedrally coordinated semiconductors have proved to be benchmarks in verifying the dielectric theory of RRS as the phonon dispersion relations and the band structures of these compounds are well known.[2–4] Conventionally, the RRS experiments are carried out by varying the incident photon energy in order to scan across the interband transition energy. However, in the view of the sensitivity of the electronic energy bands to the unit-cell volume, it is in principle possible to bring the interband transitions of a semiconductor in resonance with a fixed laser wavelength by the application of hydrostatic pressure. This pressure tuned resonance Raman scattering has been demonstrated recently in a few II-VI and III-V semiconductors[5,6] and in multiple quantum well structures.[7,8] In the present work, we report the investigation of the electronic band structure of $AgGaSe_2$ in the ambient and high-pressure phases with the help of pressure-tuned RRS. This ternary chalcopyrite I-III-VI_2 semiconductor is of considerable current interest in view of its application as a nonlinear optical material.

Tetragonal chalcopyrite I-III-VI_2 compounds are structurally correlated to the II-VI zinc-blende semiconductors.[9] Doubling of the unit cell along the c axis occurs when the divalent cation is alternately replaced by monovalent and trivalent cations. Because of cell doubling, the X and W points of the Brillouin zone fold back to the zone center and consequently, the electronic band structure and the phonon dispersion curves are most conveniently described in terms of those of the parent zinc-blende structure. Using this approach, excellent agreement between the band gaps of a similar class of ternary compounds II-IV-V_2 and the corresponding III-V binary analogs have been found.[10] On the other hand, in the case of I-III-VI_2 compounds, the band gaps are found to be considerably smaller than those of the II-VI counterparts.[11] This band-gap anomaly arises due to the hybridization of noble metal d electrons with the p electrons in the valence band.[12]

In the chalcopyrite structure, there is also a compression of the lattice (tetragonal distortion) along c axis due to ordering.[9] Further, the anion is shifted from the ideal (1/4, 1/4,1/4) position due to difference in bonding between I-VI and III-VI atoms. This anisotropy or tetragonal distortion results in a crystal-field splitting of the valence bands into light- (A) and heavy- (B) hole valence bands. Thus the spin-orbit and the crystal-field splittings lift the degeneracy of the valence band, leading to three valence bands[9] A, B, and C similar to those found in the wurtzite structure. It is seen that the spin-orbit splitting in ternary chalcopyrites is very small compared to that in II-VI compounds and is nearly zero in ternary sulphides.[13,14]

In the case of $AgGaSe_2$, c/a has a value 1.823 due to the anisotropy and the direct gap resulting from the transitions from A, B, and C valence bands at ambient temperature and pressure are seen at 1.81, 2.01, and 2.27 eV, respectively.[9] Further, the temperature dependence of the band gap is found to be anomalous and is not well understood.[15] In addition, $AgGaSe_2$ has been found to exhibit strong defect luminescence at approximately 50 meV below the free exciton energy at 2 K and the stimulated emission is also believed to be defect mediated.[16,17] Recently two defect bands have been reported in the optical absorption at ambient temperature[18] as well as in the photoluminescence at 77 K.[19] The presence of defects and the associated optical properties make $AgGaSe_2$ unique in the I-III-VI_2 chalcopyrite compounds. Recent RRS investigations at 77 K have shown resonance enhancements of $E(\Gamma_5)$ longitudinal optic (LO) phonon and its overtones and combinations at the A exciton energy.[20] High-pressure Raman investigations have revealed a sequence of three phase transitions occurring at 30, 51, and 83 kbar, respectively,[21] which have been subsequently confirmed using x-ray diffraction and the structure of the high-pressure phases have been identified.[22] A preliminary report

of the pressure-tuned resonances of the nonpolar A_1 phonon in the Raman scattering experiments has been made[23] using several fixed wavelengths of argon and krypton ion lasers of which the most interesting aspect is the observation of pressure-tuned resonances with the yellow and green wavelengths even in the high-pressure indirect-gap (opaque) phase.[21] In this paper we report the detailed study of pressure-tuned RRS in $AgGaSe_2$ and present a theoretical analysis of the resonance profiles. The pressure coefficient of the direct interband transition in the high-pressure phase is also reported.

II. EXPERIMENT

Raman spectra of unoriented single-crystal bits of $AgGaSe_2$ (100 μm size) are recorded in the backscattering geometry from a gasketed diamond anvil cell (DAC). Single crystals used in the present work were grown by R. Feigelson of Stanford university. A 16:3:1 methanol-ethanol-water mixture is used as a pressure transmitting medium. Pressure inside the DAC is estimated using the standard ruby fluorescence technique. Other details of DAC loading are described elsewhere.[24] The 676.4-, 647.1-, 568.2-, 530.9-, 520.8-, and 482.5-nm lines of krypton ion laser and 514.5- and 488.0-nm lines of argon ion laser are used to excite the Raman spectra. Laser power on the sample is kept below 10 mW to avoid heating due to resonant absorption. Scattered light from the sample is analyzed using a Spex double monochromator and detected using a cooled photomultiplier tube operated in the photon-counting mode. Scanning of the spectra and data acquisition are done using a home-built microprocessor-based data acquisition cum control system. Subsequent to the completion of a scan, data are transferred to a personal computer for further analysis.

In principle, in order to make a quantitative analysis of the intensity, one must use samples of uniform thickness. Hence the samples used for DAC loading are plateletlike with nearly uniform thickness. No extra efforts are taken to thin down the samples by grinding or polishing. Ruby fluorescence is measured using the same setup without removing the DAC from the mount, which is on a precision xy translational stage. Hence the focused laser spot on the sample in the DAC could be repositioned accurately to 10 μm while viewing with the help of a microscope. This ensures constancy of the optical path after each change of pressure and its measurement. Further, optical configuration of the experimental setup and the incident power level of a given wavelength are kept undisturbed over a pressure cycle. For each wavelength, pressure runs are repeated at least twice and the Raman mode intensities as a function of pressure are normalized to that of the peak intensity for presenting together the data from more than one run.

III. RESULTS

$AgGaSe_2$ in the tetragonal chalcopyrite phase (D_{2d}^{12}) has two formula units per unit cell and the factor group analysis predicts 15 zone center optical phonons[25]

$$\Gamma_{\text{opt}}=A_1(\Gamma_1)+2A_2(\Gamma_2)+3B_1(\Gamma_3)+3B_2(\Gamma_4)+6E(\Gamma_5)$$

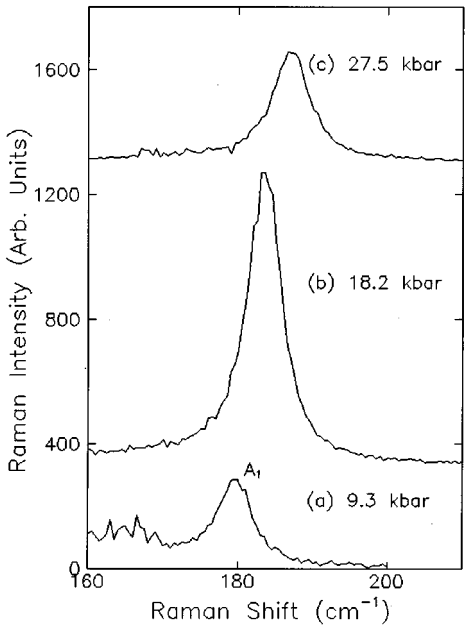

FIG. 1. Raman spectra of $AgGaSe_2$ at various pressures using the 676.4-nm line of the Kr^+ laser. The intensity of the A_1 mode depends strongly on pressure.

of which A_2 modes are Raman inactive while B_2 and E are polar phonons. Assignment of various phonons using infrared absorption and Raman spectroscopy have already been reported.[26] Recent high-pressure Raman spectroscopic measurements at ambient temperature have revealed that $AgGaSe_2$ remains in the chalcopyrite phase up to 30 kbar (Ref. 21) and the nonpolar mode of A_1 symmetry appears as the strongest mode. Figure 1 shows the Raman spectra of $AgGaSe_2$ in the A_1 mode region at different pressures in the chalcopyrite phase excited using the 676.4-nm line of the krypton ion laser. Note that the Raman intensity increases several fold as pressure is increased to about 18 kbar and subsequently decreases as the pressure is increased further. The pressure dependence of the A_1 mode peak intensity is shown in Fig. 2 for 676.4- as well as for 647.1-nm lines. Note that the Raman peak intensities pass through maxima at 18 and 30 kbar for the 676.4- and 647.1-nm lines, respectively. At the outset, one may ascribe this behavior to the pressure-tuned resonances of an electronic interband transition with the fixed energies of the incident photon. This allows one to estimate the pressure coefficient $\partial E_0/\partial P$ of the corresponding transition to be 6.9 meV/kbar. This may be compared with the values of 5.1 meV/kbar corresponding to the absorption edge due to the lowest direct gap E_g and 6.9 meV/kbar associated with the two defect levels D_1 and D_2 reported in a recent high-pressure optical absorption experiment.[18] This value of the pressure coefficient of E_g is close to the value 5.3 meV/kbar reported earlier.[27] At the ambient temperature and pressure, the defect levels D_1 and D_2 are found to lie within the band gap near the conduction band at energies 1.709 and 1.632 eV above the valence band[18] while the band gap has a value of 1.81 eV.[15] These defects are assigned to bound-to-bound transitions such as

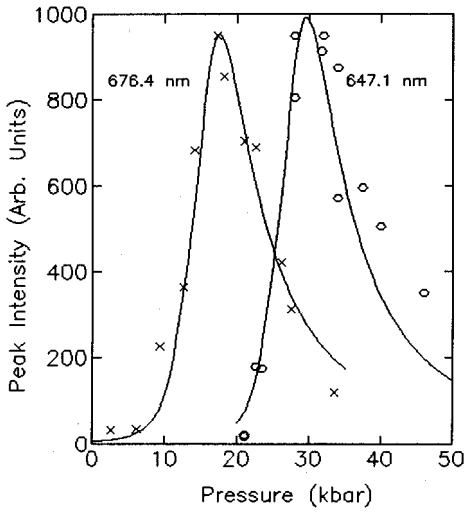

FIG. 2. Intensity of the A_1 mode as a function of pressure for the two red wavelengths of the Kr^+ laser. Solid curves are the calculated intensity profiles (see text). The rapid decrease of the intensity towards the low-pressure side is due to strong absorption.

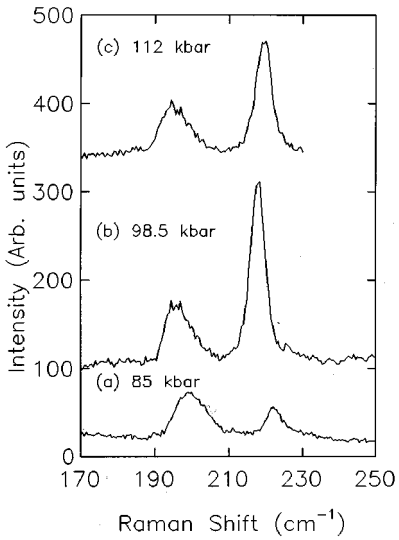

FIG. 3. Raman spectra of $AgGaSe_2$ using the 530.9-nm line of the Kr^+ laser in the orthorhombic (85 kbar) and the tetragonal phases (98.5 and 112 kbar) showing the resonance enhancement in the opaque phase. The low-frequency mode exhibits softening and its intensity does not show any noticeable dependence on pressure.

donor-acceptor pair transitions. In $AgGaSe_2$, Ga interstitials, Ga_{Ag} and Se vacancies are known donors whereas Ag vacancies act as acceptors.

In view of the closeness of the pressure coefficients of the reported defect levels D_1 and D_2 to that of the electronic transition responsible for the resonance enhancement of the A_1 mode intensity in the present experiments, it is likely that this transition is associated with one of the defect levels; however, one needs to also consider the energy of the transition before an unambiguous assignment is made. This will be discussed in further detail in the next section after the calculated resonance profiles are compared with the experimental data.

The system $AgGaSe_2$ is also reported[21] to undergo a structural phase transition when the pressure is increased beyond 30 kbar; however, the phase between 30 and 51 kbar appears to be a mixture of chalcopyrite and a new phase. The transparency of the single crystal is found to increase with increasing pressure up to 51 kbar because of the increase of the direct gap with increasing pressure. At 51 kbar the system undergoes another structural transition to a phase that is opaque to the visible light. This is probably due to a change from direct-gap to an indirect-gap semiconductor with the E_g lower than the energy of the visible photon. The behavior of phonon frequencies at high pressure suggested another transition at 83 ± 3 kbar.[21] Recent high-pressure x-ray investigations have confirmed all three structural transitions and identified the structure of some of the high-pressure phases. Combining the results of the Raman[21] and x-ray[22] investigations, the sequence of phase transitions in this system can be written as

$$\text{chalcopyrite} \xrightarrow{30\ \text{kbar}} \text{chalcopyrite} + \alpha \xrightarrow{51\ \text{kbar}} \text{orthorhombic} \xrightarrow{83\ \text{kbar}} \text{tetragonal} \xrightarrow{180\ \text{kbar}} \beta.$$

Other chalcopyrites have also shown a number of phase transitions at high pressure,[28–30] which can be compared with those in corresponding binary analogs.[31,32] This will be further discussed in detail in the next section. Another interesting aspect with this compound is that the high-pressure behaviour of this compound at 77 K appears to be significantly different from that at ambient temperature. The system does not exhibit any structural transition up to 80 kbar and the phonon frequencies exhibit a sublinear dependence on pressure.[33] This is qualitatively attributed to the decrease in compressibility at low temperatures.

The orthorhombic (opaque) phase is not found to yield any measurable Raman intensities with the red wavelengths. On the other hand, the yellow and green wavelengths give good intensities for several Raman modes. Figure 3 shows the Raman spectra in the high-pressure tetragonal phase, found above 83 kbar, at various pressures using the 530.9-nm line of the krypton ion laser. The spectrum at 85 kbar exhibits two peaks at 197 and 222 cm^{-1}. In fact, the orthorhombic and tetragonal phases are found to coexist over a pressure range of about 6 kbar around the transition pressure. In this coexistence region, the peak at 222 cm^{-1} gradually reduces in intensity and a new peak at 216 cm^{-1} appears. Subsequent increase of pressure causes the mode frequency of the 216-cm^{-1} mode to increase with pressure. On the other hand, the frequency of the 197-cm^{-1} mode continues to decrease. This soft mode was not detected in the earlier study using the 514.5-nm line of the argon ion laser probably because of a different orientation of the crystal. Figure 4 shows the behavior of these modes as a function of pressure. Note the sudden decrease of the mode frequency of the high-frequency peak and the change of slope of the soft phonon across the orthorhombic $\rightarrow$ tetragonal transition. One can also notice from Fig. 3 the several fold increase in intensity of the high-frequency mode as the pressure is increased to 98 kbar; upon further increase of pressure, the peak intensity decreases. This resonance enhancement of the

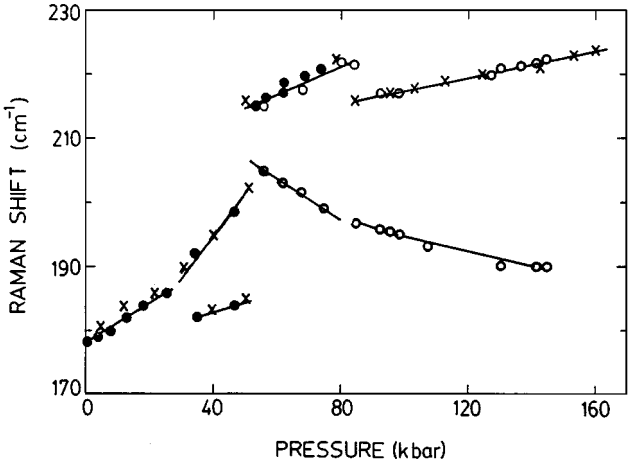

FIG. 4. Pressure dependence of the A_1 mode frequencies in $AgGaSe_2$. Different symbols correspond to different pressure runs. Phase transitions occur at 30, 51, and 83±3 kbar, respectively, which can be identified from the discontinuous changes in the phonon frequencies and their slopes.

mode intensity at around 98 kbar using the 530.9-nm line is similar to that reported earlier using the 514.5-nm line. In the present investigations, 568.2- and 520.8-nm lines of the krypton laser are also found to exhibit similar resonances, which peak at 53 and 109 kbar, respectively. Figure 5 shows the pressure dependence of the mode intensity for two green wavelengths.

The resonances observed in the high-pressure opaque phases with yellow-green wavelengths suggest pressure-tuned coincidences of some direct interband transition with fixed energies of incident photons. This also permits one to estimate the pressure coefficient of this direct interband transition to be 4 meV/kbar, which is significantly different from that observed in the chalcopyrite phase. This is expected because (a) this interband transition need not be the same as that responsible for the resonances observed in the chalcopyrite phase and (b) the pressure dependence of the electronic bands in different structures is also expected to be different. In order to obtain a more complete understanding of the electronic transitions in various phases, one needs to calculate theoretically the expected resonance profiles and compare these with the experimental data. This is done in the next section.

IV. DISCUSSIONS

Before calculating the resonance profiles, it is important to compare the phase transitions in this system with those in other chalcopyrite compounds such as $CuGaS_2$, $AgGaS_2$, $CuInSe_2$, and $AgInSe_2$ and understand their behavior and pressure-induced effects.[22,28–30] The copper compounds are found to transform to the NaCl structure from the chalcopyrite phase[28,29] while those with silver are found to exhibit a sequence of phase transitions to structures other than NaCl.[22] Comparison of phase transitions in the chalcopyrite structures with those in corresponding binary analogs is of significance in order to understand the role of various atoms in determining the structural stability and other physical properties. While the electronic properties of $CuGaX_2$ and $AgInX_2$ can be compared directly with ZnX and CdX, respectively, the electronic structure of $AgGaX_2$ is to be compared with that of the mixed crystal $Zn_{0.5}Cd_{0.5}X$ where X denotes the chalcogen atom. Many of the Zn and Cd chalcogenides are found to transform to NaCl structure at moderate pressures[31] and across this transition, the material is also found to become an indirect-gap semiconductor. However, in the mixed crystals, the sequence of phase transitions and transition pressure are found to depend on their ambient pressure structures.[32]

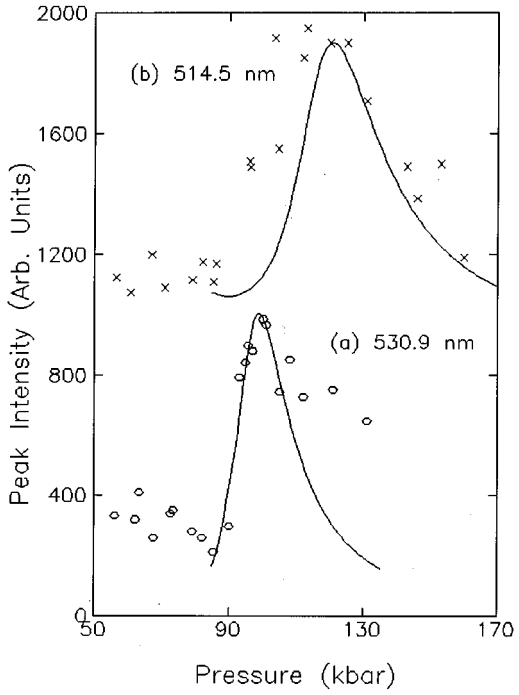

FIG. 5. Intensity of the high-frequency mode as a function of pressure for the 530.9- and 514.5-nm exciting lines. Solid curves are the calculated intensity profiles (see text).

A. Wavelength-tuned RRS

In order to calculate pressure-tuned resonance profiles, one has to first consider the general theory of wavelength-tuned RRS. The transition probability for one phonon Raman scattering can be obtained under third-order perturbation theory. Following Choi and Yu[20] one writes it as

$$R_{if}=\frac{2\pi}{\hbar}\sum_{\omega_s}\left|\sum_{nn'}\frac{\langle o|H_{er}|n'\rangle\langle n'|H_{ep}|n\rangle\langle n|H_{er}|o\rangle}{(E_n-\hbar\omega_i-i\hbar\Gamma)(E_{n'}-\hbar\omega_s-i\hbar\Gamma')}\right|^2\delta(\hbar\omega_i-\hbar\omega_s-\hbar\omega_p), \quad (1)$$

where $\hbar\omega_i$ and $\hbar\omega_s$ are the incident and the scattered photon energies, respectively, and $\hbar\omega_p$ is that of the phonon energy. Scattering can be conventionally described as a three-step process. The system in the ground state $|o\rangle$ is excited to an intermediate electron-hole pair or exciton state $|n\rangle$ by the incident photon via the electron-radiation interaction Hamiltonian H_{er}. This state $|n\rangle$ is scattered by the phonon into another intermediate state $|n'\rangle$ through the electron-phonon Hamiltonian H_{ep}. The scattered electron-hole pair recombines to give out the scattered photon bringing the system back to the ground state through the same H_{er} interaction. E_n and $E_{n'}$ are the energies of the intermediate states and Γ and Γ' are the corresponding damping constants. Although, in principle, one must sum over all the intermediate states in Eq. (1), contributions to the transition probability are significant only when the energy denominators are small, i.e., close to the resonances. When the photon energy $\hbar\omega_i$ equals that of a direct interband transition E_0, i.e., the intermediate level E_n becomes a real level with $E_n=E_0$, one observes enhancement in Raman intensities due to ''in resonance.'' On the other hand, when the scattered photon energy matches the interband transition energy E_0, enhancement in Raman intensities is observed due to ''out resonance.'' The ''out resonance'' occurs at a higher incident photon energy $\hbar\omega_i=E_0+\hbar\omega_p$. Thus in a resonance Raman experiment, as a function of incident photon energy, one expects to observe both the ''in'' and the ''out'' resonances, which are separated by the energy of the phonon $\hbar\omega_p$, both these resonances being due to the same interband transition of energy E_0. Excellent ''in'' and ''out'' resonances have been demonstrated in the case of GaSe at 77 K by Reydellet and Besson.[34]

Evaluation of the quantum mechanical matrix element is not straightforward and often one is interested only in the relative resonance profiles arising from the energy denominators. For a single direct interband transition at energy $E_0=\hbar\omega_0$ with a damping constant Γ, Eq. (1) can be simplified and rewritten as a scattering efficiency

$$S(\omega_i)=\frac{A_c}{t}\left|\frac{\omega_s^2}{(\omega_0-\omega_i-i\Gamma)(\omega_0-\omega_s-i\Gamma)}\right|^2, \tag{2}$$

where $\omega_s=\omega_i-\omega_p$ for the Stokes' scattering. Other frequency-independent terms and the matrix elements have been absorbed in the constant A_c and t is the sample thickness. S represents the ratio of the scattered to the incident intensity per unit path length within the sample and has a dimension of cm^{-1}.

The incident and the scattered radiations also undergo absorption in the sample and reflections from the surfaces. In order to account for these losses in the measured intensity, one can multiply Eq. (2) with a correction factor to obtain a dimensionless effective scattering efficiency S_{eff} as

$$S_{\text{eff}}=S(1-R_i)(1-R_s)\left\{\frac{1-\exp[-(\alpha_i+\alpha_s+S)t]}{(S+\alpha_i+\alpha_s)}\right\}, \tag{3}$$

where R_i and R_s are the reflectivities of the sample surface for the incident and the scattered photons and α_i and α_s are the corresponding absorption coefficients. These correction terms are important close to resonances because the scattering length (penetration depth) is limited by the strong absorption in the material. In order to make corrections for absorption and reflection, one must know these coefficients as a function of ω_i. These can be calculated, if the complex refractive indices are known, from the relations

$$R(\omega)=\frac{[n(\omega)-1]^2+k^2(\omega)}{[n(\omega)+1]^2+k^2(\omega)} \tag{4}$$

and

$$\alpha(\omega)=\frac{2\omega k(\omega)}{c}, \tag{5}$$

where n and k are the real and imaginary parts of the frequency-dependent complex refractive index and c is the velocity of light. The same interband transition at E_0 causes dispersion in the refractive indices in the frequency region close to resonance. In view of the lack of reported data on the refractive indices at high pressures, we calculate these from the Lorentz oscillator model for the dielectric response. The frequency-dependent real and imaginary parts of the dielectric constants are given as

$$\epsilon_1(\omega)=\epsilon_\infty+\frac{4\pi\rho\omega_0^2(\omega_0^2-\omega^2)}{(\omega_0^2-\omega^2)^2+\Gamma^2\omega^2} \tag{6}$$

and

$$\epsilon_2(\omega)=\frac{4\pi\rho\omega_0^2\Gamma\omega}{(\omega_0^2-\omega^2)^2+\Gamma^2\omega^2}, \tag{7}$$

where ϵ_∞ is the high-frequency dielectric constant and $4\pi\rho$ is the oscillator strength of the interband transition at ω_0. Although $4\pi\rho$ and ϵ_∞ can be treated as parameters, we have chosen them to be consistent with the low-frequency dielectric constant ϵ_0 ($\epsilon_0=\epsilon_\infty+4\pi\rho$), whose value was estimated to be 6.6 from the reported refractive index of the material at 13 μm.[9] The oscillator resonance frequency ω_0 and the damping constant Γ in Eqs. (6) and (7) are the same as those appearing in Eq. (2).

B. Pressure-tuned RRS

As mentioned earlier, in the present experiments, incident laser wavelengths are kept fixed during resonance profile measurements while the interband transition energy E_0 changes as the sample is subjected to high pressure. Thus ω_i are fixed and ω_0 now depends on the applied pressure P. In the chalcopyrite phase, we have also estimated the pressure coefficient of the direct interband transition energy to be 6.9 meV/kbar from the positions of the peaks in the resonance profiles obtained using the red wavelengths. As a first approximation, one can assume ω_0 to vary linearly with P in the small pressure range of 30 kbar over which the chalcopyrite phase is found to be stable. Thus we write

$$\omega_0(P)=\omega_0^{(0)}+\left(\frac{\partial\omega_0^{(0)}}{\partial P}\right)P, \tag{8}$$

where $\omega_0^{(0)}$ is the interband transition energy at ambient pressure and $\partial\omega_0^{(0)}/\partial P$ is its pressure coefficient. The value of

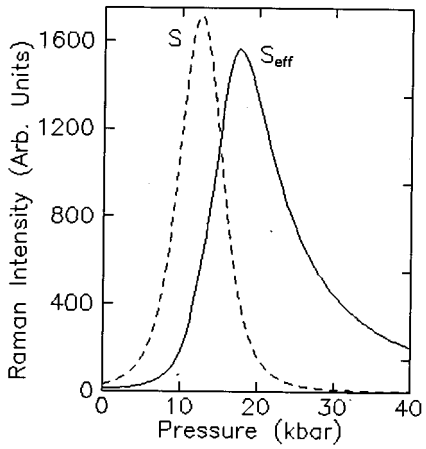

FIG. 6. Calculated pressure-tuned resonance profiles of the intensity of mode A_1 for the 676.4-nm line. The solid and the dashed curves correspond respectively to the profiles calculated with and without corrections for absorption and reflection. In order to present both the curves in the same frame, $S_{\rm eff}$ is multiplied by a factor of 700. Note the asymmetry and the shift of the peak to higher pressures due to absorption and reflection losses.

$\omega_0^{(0)}$ is estimated to be 1.736 meV from the pressure dependence of the resonance energies. The damping constant Γ, which determines the width of the resonance profile, has contributions from the intrinsic width of the transition and the temperature-dependent vibronic coupling. For the resonances with red wavelengths in the chalcopyrite phase, Γ = 31 meV is used in the calculations. In this context, it may be mentioned that a value of 11 meV for Γ at 77 K has been found to give a good fit for the wavelength-tuned resonance Raman scattering profiles.[20] Hence the value used in the present calculations is physically reasonable. Using these parameters, the pressure-tuned Raman profiles are generated for a sample thickness of 30 μm. In Eq. (3) as the attenuation due to scattering is much smaller than that due to absorption ($S \ll \alpha_i + \alpha_s$), it is neglected in comparison with the absorption coefficients. In order to understand the consequences of attenuation and reflection of the incident and scattered radiation from the sample, both S and $S_{\rm eff}$ are shown in Fig. 6. Note that S is symmetric as expected and appears in the middle of the expected positions of the ''in'' and ''out'' resonances due to large value of Γ. On the other hand $S_{\rm eff}$ is shifted to higher pressures and exhibits marked asymmetry. It is important to mention that the pressure-tuned resonance profiles can be compared with the wavelength-tuned resonance profiles if one assigns the high-pressure side of the figure to wavelengths longer than that corresponding to the resonance energy and the low-pressure side to shorter wavelengths. Thus, the absorption effects manifest themselves on the low-pressure side of the resonance profile. The rapid decrease of the Raman intensity on the low-pressure side is due to the reduction in penetration depth due to strong attenuation in the medium. The penetration depth increases monotonically as pressure is increased and saturates to a value the same as that of the thickness of the sample in the low attenuation limit. From the calculations, it is seen that if a sample of lower thickness is used, the resonance profile $S_{\rm eff}$ on the high-pressure side is less asymmetric and the peak also shifts towards that of S. Measurements carried out using red wavelengths on one such sample of smaller thickness indeed showed more symmetric profiles, which peaked at lower pressures consistent with the predictions of the calculations. The phonon frequency ω_p also changes with pressure; however, it changes ω_s only marginally and has little effect on the resonance profiles. Actually, only the oscillator strength and the damping constant are treated as parameters. The effect of increasing Γ is, in addition to the broadening of the resonance profiles, to reduce the height of the resonance peak. On the other hand, an increase in $4\pi\rho$ increases the magnitude of resonance enhancement.

TABLE I. Fit parameters and calculated and the observed resonance pressures for various wavelengths of argon and krypton ion lasers. P_s and P_e correspond to the peaks in the resonance profiles S and $S_{\rm eff}$. P_m is the position of the experimental resonance profile.

λ (nm)	$4\pi\rho$	Γ (meV)	P_s (kbar)	P_e (kbar)	P_m (kbar)
676.4	1.0	31	14	17	18 ± 1
647.1	1.0	31	26	29	30 ± 1
568.2	0.7	35	53	59	53 ± 3
530.9	0.7	35	91	99	98 ± 2
520.8	0.7	35	103	109	110 ± 2
514.5	0.7	60	110	121	120 ± 5

The calculated resonance profiles for the 676.4- and 647.1-nm lines using the parameters discussed above are also shown in Fig. 2 as continuous curves. It is gratifying to note the excellent agreement between the experimental and calculated profiles with just two parameters. It may be mentioned that although the Lorentz oscillator model corrects for absorption and reflection and accounts for the intensity profile reasonably close to resonance, it fails to correctly predict the intensities away from the resonance, especially at low pressures. This is because, in the Lorentz model, absorption decreases monotonically to zero at much lower pressures (or equivalently, at photon energies much higher than that of the resonance), whereas in the actual sample, absorption remains high for all lower pressures (or, equivalently, for all higher photon energies). This leads to an apparent increase of the calculated intensities far away from resonance. The parameters used in the fitting for various wavelengths are given in Table I and also the observed resonance pressures along with those obtained from the calculated resonance profiles. As mentioned earlier, the resonance profiles are expected to peak when $\omega_i = \omega_0(P_s) + \omega_p/2$; i.e., resonance will occur at pressure P_s given as

$$P_s = (\omega_i - \omega_0^{(0)} - \omega_p/2)\left(\frac{\partial\omega_0^{(0)}}{\partial P}\right)^{-1}. \tag{9}$$

However, the resonance profile, when corrected for absorption and reflection losses, is shifted to higher pressures and one finds excellent agreement between the pressure P_e of the peak in $S_{\rm eff}$ and the actually observed resonance peak pressure P_m.

As mentioned earlier, when the pressure is increased beyond 51 kbar, the sample turns opaque, suggesting discontinuous changes in the band structure across the structural

transition to the orthorhombic phase. In view of the lack of information about the dielectric constant in the high-pressure phases and in order to keep the number of adjustable parameters to a minimum, ϵ_0 in the high-pressure phase is taken to be the same as that in the chalcopyrite phase. The pressure dependence of the direct interband transition in the high-pressure phase used in the fitting is

$$\omega_0(P)=\omega_0^{(51)}+(P-51)\frac{\partial\omega_0^{(51)}}{\partial P}, \tag{10}$$

where $\omega_0^{(51)}=2.174$ eV is the energy of the interband transition in the orthorhombic phase at 51 kbar. The pressure coefficient $\partial\omega_0^{(51)}/\partial P$ has a value of 4 meV/kbar. For most of the green wavelengths, reasonably good agreement between the calculated and the observed profiles is seen with $4\pi\rho=0.7$ and a value of Γ larger than that of the chalcopyrite phase. These parameters are also given in Table I. The calculated resonance profiles for the 530.9- and 514.5-nm lines are also shown in Fig. 5 as continuous curves. Note that the apparent rise of the calculated profile for 514.5 nm line towards the low-pressure side is because of the insufficient correction for the absorption losses as pointed out earlier. It is reasonable to expect an increase in the intrinsic width of the electronic transitions at high pressures, resulting in a higher value of Γ and a corresponding broadening of the resonance profiles as is seen in the case with the 514.5-nm line. Agreement between the peak positions in the calculated and the observed profiles is also good. The agreement between the experimental and the calculated profiles on the high-pressure side being not so good is probably because of the absorption due to the indirect gap, which is not accounted for by the Lorentz model. Figure 7 shows the plot of the observed and the fitted values of the interband transition energies as a function of pressure. The dashed line shows the peak position of the S profile and the shift of observed resonances to higher pressures due to absorption and reflection effects is clearly seen. Note the discontinuous increase of about 125 meV in the direct interband transition energy across the transition at 51 kbar. Such discontinuous changes in the band structure are expected across a structural transition and the pressure-tuned RRS studies have allowed one to probe these in the high-pressure phases. It may be mentioned that a resonance with the 488.0-nm line is expected at around 155 kbar; however, no significant variation in the mode intensity as a function of pressure was seen with this wavelength. This may be due to the effect of a decreased penetration depth of the radiation arising from a larger indirect gap absorption and also due to the increased Γ as the pressure-induced metallization is approached.

Having obtained the direct interband transition energies and their pressure dependencies, one can now attempt assigning these. Note that the transition energy $\omega_0^{(0)}=1.736$ eV is close to that of the defect level D_1 (1.709 eV) observed by Choi and Yu.[18] As mentioned earlier, the reported pressure coefficient of this defect level also agrees well with that observed from the present studies. Hence the electronic transition responsible for the resonance enhancement of the A_1 mode in the chalcopyrite phase can be assigned to that of the defect level D_1. The appearance of resonance Raman peak positions at 20–30 meV higher than the direct interband transition energies obtained from optical measurements is well known in zinc-blende semiconductors.[35] However, the reason for this shift is not well understood.[36] As this defect level has a larger pressure coefficient than that of the band gap E_g, it merges with the conduction band at pressures slightly below 51 kbar. In view of this, the direct interband transition causing resonances with the yellow and green wavelengths in the high-pressure opaque phase can be assigned to the direct gap in those phases. The discontinuity seen in Fig. 7 thus corresponds to a change in the direct gap E_0 across the structural transition at that pressure. A lower value of the pressure coefficient of the direct gap is also consistent with its assignment. Although one expects changes in the band structure across the orthorhombic $\rightarrow$ tetragonal transition, no noticeable changes in the direct interband transition energy are detected. In order to obtain the pressure dependence of E_0 in the orthorhombic phase one needs several wavelengths exhibiting resonances between 51 and 83 kbar. Because of the availability of only one line in this region, precise identification of possible discontinuity across the orthorhombic-tetragonal transition could not be done in the present experiments.

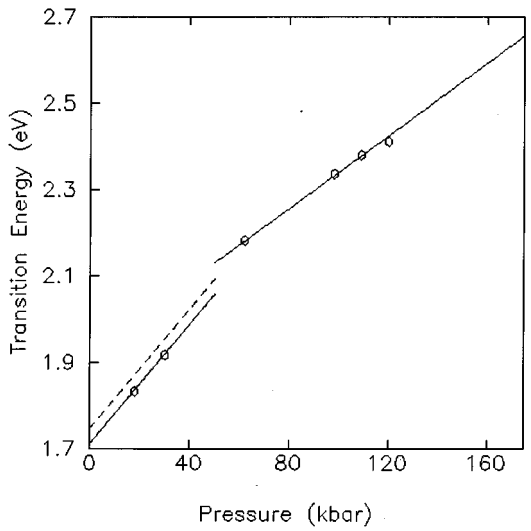

FIG. 7. The direct interband transition energy in $AgGaSe_2$ as a function of pressure in chalcopyrite and other high-pressure phases. The dashed line represents the position of the peak (P_s) in the calculated profiles S. Solid line is the peak position (P_e) of the profile S_{eff}. Data points corresponds to the six wavelengths used in the study and the corresponding resonance pressure values (P_m). Note that the solid line is shifted to the right with respect to the dashed line as expected. A discontinuous increase of 125 meV in the direct gap arises across the structural transition at 51 kbar (see text).

It is worth comparing the present pressure-tuned RRS with those of the wavelength-tuned RRS carried out by Choi and Yu at 77 K.[20] In these measurements also, the resonance of the A_1 mode exhibits a clear asymmetry and the resonance energy is shifted to a lower photon energy as compared to the exciton energy. These observations are in perfect agreement with the present arguments about the consequences of absorption and reflection losses. On the other hand the $E(\Gamma_5)$ LO phonon is found to exhibit a much stronger resonance, which occurs at $1s$ exciton energy, than the $A_1(\Gamma_1)$

phonon. This is because of the strong LO-phonon–1s exciton coupling arising from the Fröhlich interaction whereas in the case of $A_1(\Gamma_1)$, it is only the deformation potential through which it interacts with the electron-hole pair. It may be mentioned that in the chalcopyrite phase no resonances are observed due to the direct gap E_g. In fact, for the photon energy corresponding to the 676.4-nm line, resonance with E_g is expected at pressures very close to the ambient pressure. The reason for this is not clear at present. On the other hand, observation of strong resonances with the defect level D_1 is probably because it gets populated by carriers at ambient temperature. Further work is necessary to completely characterize these defect levels.

V. CONCLUSIONS

To conclude, we have been able to probe the behavior of electronic interband transitions in the chalcopyrite and other high-pressure indirect-gap phases. The direct interband transitions giving rise to these resonances in these phases are assigned to a defect level and to the direct gap, respectively. The pressure coefficient of the defect level in the chalcopyrite phase is estimated to be 6.9 meV/kbar and that of the E_0 gap in the opaque phase is 4 meV/kbar. The change in direct gap across the structural transition at 51 kbar is estimated to be 125 meV. Broadening of the resonance profiles at high pressures suggests an increase in the intrinsic width of the electronic energy bands due to overlap.

ACKNOWLEDGMENTS

It is a pleasure to acknowledge Professor L. Artús of Consell Superior d'Investigacions Cientifiques, Barcelona for the gift of the single crystals used in the present work. The authors also thank Dr. Kanwar Krishan for his keen interest in the work and Dr. Baldev Raj and Dr. P. Rodriguez for encouragement.

[1] M. Cardona, in *Light Scattering in Solids II*, edited by M. Cardona and G. Güntherodt (Springer, Berlin, 1982), p. 19.
[2] J.E. Zucker, A. Pinczuk, D.S. Chemla, A. Gossard, and W. Wiegmann, Phys. Rev. Lett. **53**, 1280 (1984).
[3] R.M. Martin and C.M. Varma, Phys. Rev. Lett. **26**, 1241 (1971).
[4] R. Trommer and M. Cardona, Phys. Rev. B **17**, 1865 (1978).
[5] P.Y. Yu and B. Welber, Solid State Commun. **25**, 209 (1978).
[6] A.K. Arora and A.K. Ramdas, Phys. Rev. B **35**, 4345 (1987).
[7] M. Holtz, U.D. Venkateswaran, K. Syassen, and K. Ploog, Phys. Rev. B **39**, 8458 (1989).
[8] A. Jayaraman, G.A. Kourouklis, R. People, S.K. Sputz, R.G. Maines, Sr., D.L. Sivco, and A.Y. Cho, High Pressure Res. **6**, 27 (1990).
[9] J.L. Shay and J.H. Wernick, *Ternary Chalcopyrite Semiconductors: Growth, Electronic Properties and Applications* (Pergamon, New York, 1975).
[10] J.L. Shay and E. Buehler, Phys. Rev. Lett. **26**, 506 (1971).
[11] J.L. Shay and H.M. Kasper, Phys. Rev. Lett. **29**, 1162 (1972).
[12] J.E. Jaffe and A. Zunger, Phys. Rev. B **29**, 1882 (1984).
[13] B. Tell, J.L. Shay, and H.M. Kasper, Phys. Rev. B **4**, 2463 (1971).
[14] J.L. Shay, B. Tell, H.M. Kasper, and L.M. Schiavone, Phys. Rev. B **7**, 4485 (1973).
[15] L. Artús and Y. Bertrand, Solid State Commun. **61**, 733 (1987).
[16] B. Tell and H.M. Kasper, Phys. Rev. B **4**, 4455 (1971).
[17] J.L. Shay, B. Tell, and H.M. Kasper, Appl. Phys. Lett. **19**, 366 (1971).
[18] I.-H. Choi and P.Y. Yu, Appl. Phys. Lett. **64**, 1717 (1994).
[19] I.-H. Choi and P.Y. Yu, J. Phys. Chem. Solids **56**, 595 (1995).
[20] I.-H. Choi and P.Y. Yu, Phys. Rev. B **49**, 16 407 (1994).
[21] A.K. Arora, T. Sakuntala, and L. Artús, J. Phys. Chem. Solids **54**, 381 (1993).
[22] T. Tinoco, A. Polian, J.P. Itie, E. Moya, and J. Gonzalez, J. Phys. Chem. Solids, **56**, 481 (1995).
[23] T. Sakuntala and A.K. Arora, in *Proceedings of the XIV International Conference on Raman Spectroscopy*, edited by N.-T. Yu and X.-Y. Li (Wiley, Chichester, 1994), p. 368.
[24] A.K. Arora and T. Sakuntala, Solid State Commun. **75**, 855 (1990).
[25] J. Cammassel, L. Artús, and J. Pascual, Phys. Rev. B **41**, 5717 (1990).
[26] L. Artús, J. Pujol, J. Pascual, and J. Cammassel, Phys. Rev. B **41**, 5727 (1990).
[27] A. Jayaraman, V. Narayanamurti, H.M. Kasper, M.A. Chin, and R.G. Maines, Phys. Rev. B **14**, 3516 (1976).
[28] C. Carlone, D. Olego, A. Jayaraman, and M. Cardona, Phys. Rev. B **22**, 3877 (1980).
[29] J. Gonzalez, M. Quintero, and C. Rincon, Phys. Rev. B **45**, 7022 (1992).
[30] A. Jayaraman, P.D. Dernier, H.M. Kasper, and R.G. Maines, High Temp. High Press. **9**, 97 (1977).
[31] S. Ves, U. Schwarz, N.E. Christensen, K. Syassen, and M. Cardona, Phys. Rev. B **42**, 9113 (1990).
[32] A.K. Arora and T. Sakuntala, Phys. Rev. B **52**, 11 052 (1995).
[33] I.-H. Choi and P.Y. Yu, Solid State Commun. **90**, 345 (1994).
[34] J. Reydellet and J.M. Besson, Solid State Commun. **17**, 23 (1975).
[35] R. Carles, N. Saint-Cricq, J.B. Renucci, A. Zwick, and M.A. Renucci, Phys. Rev. B **22**, 6120 (1980).
[36] M. Rösch, R. Atzmüller, G. Schaack, and C.R. Becker, Phys. Rev. B **49**, 13 460 (1994).